Response characteristics of drill-string guided wave in downhole acoustic telemetry

Ao-Song Zhao(赵傲耸)[1,2], Hao Chen(陈浩)[1,2,3,†], Xiao He(何晓)[1,2,3], Xiu-Ming Wang(王秀明)[1,2,3], and Xue-Shen Cao(曹雪砷)[1,3]

[1] *State Key Laboratory of Acoustics, Institute of Acoustics, Chinese Academy of Sciences, Beijing* 100190, *China*
[2] *University of Chinese Academy of Sciences, Beijing* 100049, *China*
[3] *Beijing Engineering Research Center of Sea Deep Drilling and Exploration, Institute of Acoustics, Chinese Academy of Sciences, Beijing* 100190, *China*

(Received 25 April 2022; revised manuscript received 29 July 2022; accepted manuscript online 2 September 2022)

Modeling of a drill-string acoustic channel has been an important topic in downhole telemetry for a long time. The propagation of drill-string guided waves in the borehole contains excitation, attenuation, and mode conversion issues that have not been considered by existing modeling methods. In this article, we formulate a hybrid modeling method to investigate the response characteristics of a fundamental-mode drill-string wave in various borehole environments. This hybrid method provides channel functions, including transmitting and receiving deployments, periodicity of the structure, and formation property changes. The essential physics of the drill-string wave propagation is captured with a one-dimensional model. The analytical solutions of the wavefield in multilayered cylindrical structures are introduced into a propagation matrix to express drill-string-wave interactions with the borehole environments. The effectiveness of the proposed method is confirmed through comparison with the finite-difference method. In addition, by designing numerical models, we investigate the conversion effect of the drill-string wave at the tool joint. We demonstrate that the conversion intensity of the drill-string wave is positively correlated not only with the cross-sectional area of the tool joint but also with the wave impedance of the outer formation. Hard formation outside the borehole reduces the energy leakage while intensifying the conversion of drill-string waves to Stoneley waves, and the opposite is true for the drill string in an infinite fluid. The converted Stoneley waves interfere with the drill-string waves, resulting in variations of bandgap distribution, which challenges the reliability of the data transmission.

Keywords: downhole acoustic telemetry, drill-string wave, bandgap characteristic, mode conversion

PACS: 43.20.+g, 91.60.Lj, 47.11.Bc **DOI:** 10.1088/1674-1056/ac8e98

1. Introduction

Effective communication between downhole and surface instruments has become a critical need in logging while drilling (LWD) operations since real-time acquisition and interpretation of downhole data streams enable engineers to mitigate drilling risks and to optimize well placement and the overall rate of penetration. Since cable transmission is unavailable during drilling, a downhole acoustic telemetry (DAT) system using the drillstring guided wave can be a prospective alternative.[1–4] Strong scattering occurs when the drill-string guided wave passes through periodically arranged tool joints, which in turn leads to frequency selective fading, also known as the band-gap characteristic. Accurate modeling of the downhole drill-string channel has been an important topic for a long time. Many researchers proposed approximation methods based on the one-dimensional (1-D) phononic crystal theory. Drumheller *et al.*[5–7] developed a time-domain finite-difference algorithm to simulate the drill-string acoustic response. Also, researchers theoretically investigated the vibration properties of fundamental-mode drill-string waves and validated the rationality of the 1-D approximation, especially in weak-dispersion areas.[8,9] The analytical methods in the frequency domain were reported afterward due to the computational efficiency and flexibility. Lous *et al.*[10] and Wang *et al.*[11] proposed two-port propagation matrix methods to evaluate the reflection and transmission coefficients. In addition, using the fourth-order Runge–Kutta technique, Carcione *et al.*[12] developed a time-domain algorithm for propagation of low-order axial, torsional, and flexural stress waves. The method was able to approximate various losses of drill-string waves by introducing several viscoelastic models.

The existing algorithms can predict the band-gap distribution when the drill string is measured in air, as illustrated by data from some ground tests.[13,14] However, transmission environments in the borehole are more complex. With reference to studies on the LWD wavefield, the impacts of the outer formation on the borehole guided wave are of interest, especially regarding the mechanisms of wave excitation, attenuation, and conversion. Cui[15] and Sinha *et al.*[16] revealed the coupling between the collar and borehole. Zheng *et al.*[17] presented that the attenuation and excitation spectra of the collar wave are significantly affected by the formation property. He *et al.*[18] revealed that reflection echoes from the borehole wall

†Corresponding author. E-mail: chh@mail.ioa.ac.cn

© 2023 Chinese Physical Society and IOP Publishing Ltd

can produce indirect collar waves, which made the LWD wave fields more complex. For the acoustic isolator in LWD, Yang *et al.*[19] found that grooves on the surface of a drill collar extended the duration of the collar wave and converted part of the collar-wave energy into long-duration Stoneley wavetrains. The Stoneley wave is the interfacial wave propagating along the fluid-solid interfaces in the borehole. Its speed is close to the fluid acoustic velocity. Since the structure of the LWD isolator is also axially periodic, just like a short drill string, the wavefield variations caused by grooving are instructive for our issue. To measure actual channel responses, Drumheller *et al.*[6,7] conducted hundreds of heavy hammer tests at 1500 m well depth. The provided data showed that the hammer excited both the drill-string wave and the mud pulse (i.e., Stoneley wave) in the borehole. The spectra transformed from impulse responses indicated that the actual passband positions always deviated a little from the theoretical calculations. In addition to this, we noted that the time delay spread of the impulse response was several times larger than the estimated result. As the Stoneley-wave speed is only 1/3 of that of the drill-string wave, it is reasonable to speculate that a portion of drill-string waves has converted to Stoneley waves, resulting in a long delay in the downhole channel. However, the mechanism of drill-string-wave conversion has not been theoretically discussed. In the absence of systematical investigations of the excitation, attenuation, and mode conversion effects, the complexity of the drill-string wavefield in the borehole can be seriously underestimated, which leaves the simulation results inconsistent with the actual data.

Although the existing 2-D finite difference method addressing the borehole wavefield provides reliable simulation results, it is too computationally inefficient as communication modeling and suffers from numerical instability due to absorption boundaries when receiving signals for long periods. Moreover, the commonly used 1-D modeling algorithm only considers the case of a free drill string and ignores its coupling with the fluid-filled borehole, so it cannot reflect the change in the radial waveguide environment. In this article, we establish a physical model of DAT and propose a hybrid modeling method to simulate the drill-string-wave response. By combining the mode wavenumber and excitation function of the drill-string wave, this hybrid method involves both the interaction of radial medium changes and the axial periodicity of the drill-string structure. The suitable deployment of the source and receiver array is determined by calculating excitation functions in frequency and spatial domains. Then the accuracy of the hybrid method is verified by comparing the simulation results with the 2-D finite-difference method. The mechanism of radial leakage is revealed by applying radially infinite media with different acoustic impedances. Finally, various numerical models are designed to evaluate the conversion intensity of the drill-string wave at the tool joint, and the bandgap variations are observed.

2. Theoretical basis

The DAT system can be modeled as a concentric cylindrically layered structure, as shown in Fig. 1. The radial layers from inside to outside of the borehole are the fluid in the drill string, the steel drill string, the fluid outside the drill string, and the radially infinite formation, respectively. The drill string consists of a periodic cascade of drill pipes and tool joints, and the ends of the drill string are assumed to be an infinite length in the z-direction. We define an (r, z) cylindrical coordinate system and let the borehole axis coincide with the z-axis, as depicted in Fig. 1. Moreover, an annular source is mounted on the outer wall of the drill pipe and the axial position corresponds to $z = 0$.

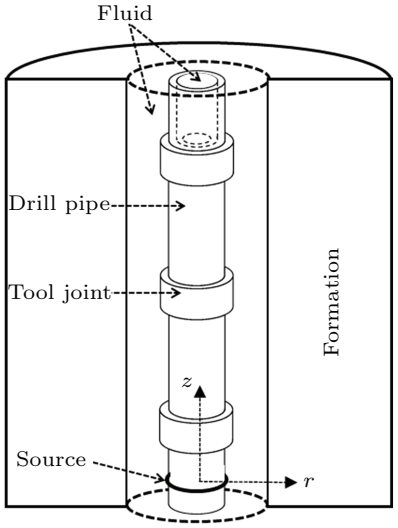


Fig. 1. The sketch of a radially layered model for the DAT at the (r, z) cylindrical coordinates. From inside to outside, the four layers are the fluid within the drill string, the steel drill string, the fluid out of the drill string, and the formation, respectively. The drill string consists of a periodic cascade of drill pipes and tool joints.

The evaluation of the drill-string channel function is divided into two steps. Firstly, for the case of a uniform drill string, the borehole wavefield is calculated to obtain the fundamental-mode drill-string wavenumber and excitation function. The physical model is a 2-D cylindrical multilayered structure where the changes in the drill-string diameter are neglected. Then the problem is approximated to the 1-D propagation to reflect the periodicity of the drill string on the z-axis. The mode wavenumber and excitation function are substituted into propagation matrices to construct a hybrid algorithm involving the transmitting and receiving deployments, periodicity of the structure, and formation property variations.

2.1. Dispersion and excitation of drill-string wave

For theoretically evaluating the mode dispersion and excitation, it is necessary to treat the drill string as a uniform long

pipe and ignore the periodic tool joints. In this case, the physical model becomes a multilayered cylindrical structure with uniform surfaces, which is equivalent to the acoustic LWD. The dispersion properties can be obtained by the dispersion equation, which can be derived as[15,16]

$$|\boldsymbol{D}(k,\omega,r)| = 0, \tag{1}$$

where k is the axial wavenumber of the wave mode; ω is the angular frequency; r refers to the radial distance of each interface. $\boldsymbol{D}$ is the matrix representing the wavefield of a multilayered cylindrical structure, and the detailed mathematical expression for the matrix $\boldsymbol{D}$ has been given by Cui.[15] In particular, R_1, R_2, and R_3 are the inner and outer radii of the drill string and the borehole radius, respectively. For the case of a drill string in an infinite fluid (i.e., $R_3 = \infty$), the dispersion equation can be similarly obtained.

In order to evaluate the excitation characteristic, the source is introduced in the form of a boundary condition

$$\tau_{zr(2)} = \sigma_{\rm s}, \quad \text{at} \ \ r = R_2, \tag{2}$$

where the field quantity $\tau_{zr(2)}$ denotes the shear stress components at the outer radius of the drill string; the symbol $\sigma_{\rm s}$ in Eq. (2) denotes the shear-stress source applied at the outer pipe wall. Because of the axial vibration property of the fundamental-mode drill-string wave, especially at a weak-dispersion low-frequency area, this loading approach is suitable for our issue.[20,21]

For the problem of solving the complex-valued roots of Eq. (1), root finding can be performed by the Newton iteration method. By solving Eq. (1), the poles of guided wave modes can be evaluated, and the drill-string wave arrival is contributed by the pole of the wavefields in the complex wavenumber plane.[22] The excitation function can be evaluated by calculating the residues of the field components at the poles of the drill-string mode wave.[18] Since receivers are generally exposed to fluid, it is appropriate to receive the normal stress component τ_{rr}. The excitation intensity with frequency ω_0 at the point (r_0, z_0) can be obtained by

$$E(\omega_0, r_0, z_0) = \frac{{\rm i}{\rm e}^{{\rm i}k_{\rm d}(\omega_0)z_0} \cdot \tau_{rr(n)}[\omega, k_{\rm d}(\omega_0), r_0]}{\partial |\boldsymbol{D}(\omega,k,r)|/\partial k|_{k=k_{\rm d}(\omega_0)}}, \tag{3}$$

where $k_{\rm d}(\omega_0)$ denotes the pole, i.e., the solution to Eq. (1), corresponding to the drill-string wavenumber at any frequency $\omega = \omega_0$; ${\rm i} = \sqrt{-1}$; the subscript number (n) denotes the layer index from inside to outside.

The time-domain waveform received at the point (r_0, z_0) can be obtained by the Fourier transform

$$e(t, r_0, z_0) = \frac{1}{2\pi}\int_{-\infty}^{+\infty}[E(\omega, r_0, z_0)\cdot S(\omega)]{\rm e}^{{\rm i}\omega t}{\rm d}\omega, \tag{4}$$

where $S(\omega)$ is the source spectrum.

2.2. Hybrid modeling method

The drill-string wave used for DAT is a single-mode guided wave in the low-frequency weak-dispersion band. Rama Rao *et al.*[9] has demonstrated that the drill-string wave was characterized by axial displacements and stresses that are uniform over the cross section of the pipe in this band. Moreover, the drill-string radius changes and coupling of surrounding formation can both be attributed to the mode wavenumber, and the near-field excitation function reflects the source effect. Under these conditions, solving the problem in a case of 1-D propagation is sufficient.

As illustrated in Fig. 2, the drill string is composed of N elements. $\Phi_{\rm I}$, $\Phi_{\rm R}$, and $\Phi_{\rm T}$ denote the amplitudes of the incident, reflected, and transmitted waves, respectively. For a 1-D plane wave propagating along the z-direction, the displacement potential is given by

$$\varphi_z = (\Phi_{\rm i}{\rm e}^{{\rm i}k_{\rm d}(\omega)z} + \Phi_{\rm r}{\rm e}^{-{\rm i}k_{\rm d}(\omega)z}){\rm e}^{{\rm i}\omega t}, \tag{5}$$

where $\Phi_{\rm i}$ and $\Phi_{\rm r}$ denote the amplitudes of the potential function of incident waves and reflected waves, respectively; $k_{\rm d}(\omega)$ is the mode wavenumber calculated by Eq. (1) and should be evaluated separately for the drill pipe and the tool joint sections; ${\rm e}^{{\rm i}\omega t}$ is the simple harmonic term of time and will be omitted in the subsequent derivation. By introducing the mode wavenumber, 1-D waves can also interact with the radial multilayered waveguide.

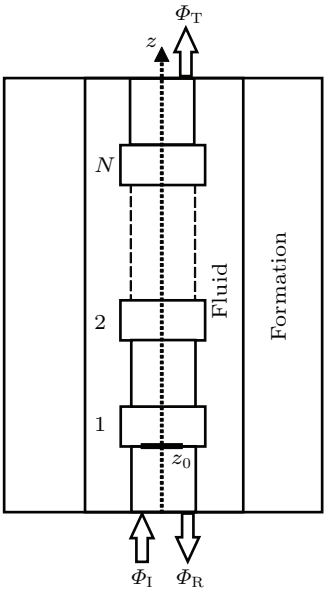


Fig. 2. The drill string contains N tool joints. $\Phi_{\rm I}$, $\Phi_{\rm R}$, and $\Phi_{\rm T}$ denote the amplitudes of the incident, reflected, and transmitted waves, respectively.

Following Wang *et al.*,[11] we adopt the continuity conditions of axial displacement u_z and force F at the interfaces. Take the interface $z = z_0$ as an example, and we can obtain

$$u_z(z_0^-) = u_z(z_0^+), \tag{6}$$

$$F(z_0^-) = F(z_0^+), \tag{7}$$

with

$$u_z = \frac{\partial \varphi_z}{\partial z}, \tag{8}$$

$$F = -EA\frac{\partial u_z}{\partial z}, \tag{9}$$

where E is the Young modulus, and A is the cross-sectional area. Then, by repeatedly applying the above continuity conditions at the periodic interfaces, we can obtain the propagation equation of the drill string as follows:[11]

$$\begin{bmatrix} \Phi_{\mathrm{I}} \\ \Phi_{\mathrm{R}} \end{bmatrix} \cdot M_N = \begin{bmatrix} \Phi_{\mathrm{T}} \\ 0 \end{bmatrix}, \tag{10}$$

where M_N is the propagation matrix. The transmission coefficient $T(\omega, z)$ is defined as

$$T(\omega, z) = \frac{\Phi_{\mathrm{T}}}{\Phi_{\mathrm{I}}}. \tag{11}$$

The incident wave Φ_{I} is related to the source and the excitation function. At a near-source position, it is given by $\Phi_{\mathrm{I}}(\omega) = E(\omega, r_0, z_{\mathrm{s}}) \cdot S(\omega)$, where $E(\omega, r_0, z_{\mathrm{s}})$ is the near-field excitation function obtained from Eq. (3), $z = z_{\mathrm{s}}$ is the axial position near the source, and $S(\omega)$ is the source spectrum. The transmitted wave is then transformed into the time domain using an inverse Fourier transform

$$\Phi_{\mathrm{T}}(t, z) = \frac{1}{2\pi}\int_{-\infty}^{+\infty} [T(\omega, z) \cdot E(\omega, r_0, z_{\mathrm{s}}) \cdot S(\omega)] \mathrm{e}^{\mathrm{i}\omega t} \mathrm{d}\omega. \tag{12}$$

Equations (11) and (12) are the frequency-domain and time-domain responses of the drill-string wave, respectively. The near-field excitation function is used as an input to the drill-string channel response, and the receiving deployment needs to be determined based on the amplitude distribution in the spatial domain.

3. Results and discussion

The model parameters used for simulations are listed in Table 1. It should be noted that the radius parameter refers to the outer radius of each layer. The P velocity refers to the velocity of the primary (P) wave or compression wave in each medium. The S velocity refers to the velocity of the secondary (S) wave or shear wave in each medium. We design three waveguide environments to study their interaction with the drill-string wave, namely, hard and soft formation boreholes and infinite fluid. Formations are classified according to acoustic impedance. The hard formation has significantly greater acoustic impedance than the soft formation, both for compression and shear waves. The acoustic impedances of formations are much larger than that of an infinite fluid. The case of the drill string in an infinite fluid can simulate acoustic telemetry in deep-sea drilling. The drill string consists of a certain number of standard 4-in drill pipes, each with a length of 5 m. In addition, we design three types of tool joints with increasing outer radii in sequence while keeping the inner radius the same as the drill pipe. The length of all three types of tool joints is set to 0.2 m.

Table 1. Model parameters for the simulations.

	Density (kg/m^3)	P velocity (m/s)	S velocity (m/s)	Radius (m)	Length (m)
Fluid within drill pipe	1000	1470	–	0.042	∞
Drill pipe	7800	5860	3130	0.050	5.0
Fluid out of drill pipe	1000	1470	–	0.120/∞	∞
Hard formation	2320	3972	2455	∞	∞
Soft formation	2485	2590	1067	∞	∞
Tool joint 1	7800	5860	3130	0.060	
Tool joint 2	7800	5860	3130	0.070	0.2
Tool joint 3	7800	5860	3130	0.080	

3.1. Excitation and attenuation characteristics of the drill-string wave

Without tool joints, the excitation and attenuation characteristics of the drill-string wave in the DAT model can be theoretically studied. Taking the borehole surrounded by hard formation as an example, we first investigate the energy distribution of the drill-string wave in each radial layer. Figure 3(a) presents excitation amplitudes in different radial positions at the three selected frequency points. The amplitudes here mean the absolute value of the radial normal stress component calculated by Eq. (3). Each plot in Fig. 3(a) is normalized concerning its maximum value for the convenience of observation and comparison. The receiver-to-source offset z_0 is set to 500 m. Figure 3(a) reveals that the drill-string wave spreads through the entire layering structure. As the wave travels forward, energy continuously leaks out into the infinite radial formation. From the three plots, excitation amplitudes mostly concentrate in the inner fluid cylinder. Further, by collecting the excitation amplitudes of the inner and outer surfaces of the drill string at the fixed axial position, two excitation spectra are obtained, as shown in Fig. 3(b). From the ratios labeled in Fig. 3(b), the excitation amplitudes of the inner surface are several times larger than those of the outer surface throughout the whole frequency range. This property means that mounting receivers at the inner surface of the drill string can achieve stronger drill-string waves, which will be a guideline in the subsequent modeling. Similar results can be obtained in the cases of an infinite fluid

and a soft formation and will not be re-discussed here.

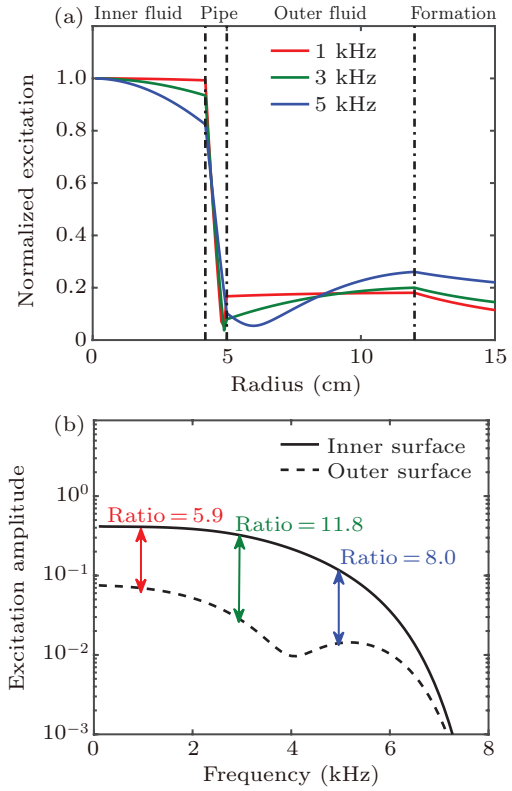


Fig. 3. The excitation amplitudes of the drill-string wave in a hard formation. The receiver-to-source offset is $z_0 = 500$ m. (a) Normalized excitation amplitudes in different radial positions at three selected frequencies. (b) The comparison of excitation spectra received at the inner surface $r_0 = R_1$ (solid line) and the outer surface $r_0 = R_2$ (dashed line), respectively. The double-sided arrows represent the ratio of the excitation amplitudes on the outer surface to that on the inner surface at three selected frequencies.

After determining the suitable receiving deployment (i.e., $r_0 = R_1$), we calculate the excitation amplitudes received at the near-source position and also give the results for the far field as a comparison in Fig. 4(a). The results for the three cases are given in Fig. 4(a), where the solid lines indicate excitation amplitudes received at $z_0 = 3$ m, and the dashed lines correspond to $z_0 = 500$ m. It is illustrated that the excitation property of the drill-string wave near the source is hardly affected by the surrounding media. In addition, the excitation spectra at the near-source position are very uniform in the frequency band of our interest, which indicates that the source is loaded appropriately, referring to Eq. (2). By comparing the results with those received at $z_0 = 500$ m, it is found that the coupling between the borehole environment and the drill-string wave is mainly reflected in the radial energy leakage. Figure 4(b) presents attenuation curves calculated by

$$\alpha(\omega) = 1000 \times 20 \log_{10} \mathrm{e}^{\mathrm{Im}[k_{\mathrm{d}}(\omega)]}. \tag{13}$$

In these open waveguides, the drill-string wave continuously leaks energy into the infinite radial media during propagating, which is the physical mechanism of attenuation. Table 2 lists several attenuation values recorded from Fig. 4(b) at three selected frequencies. According to Table 2, the values corresponding to the borehole are much lower than those of the infinite fluid. Specifically, the attenuation caused by hard formation at 1 kHz is only less than 1/10 of that caused by infinite fluid. Although the value of the soft formation at 1 kHz is close to that of the infinite fluid case, the difference gradually increases as the frequency increases. Therefore, outermost media with large acoustic impedance can significantly reduce the leakage of wave energy. Based on this understanding, it is revealed that the borehole surrounded by formations is more favorable for the long-distance propagation of drill-string waves than the infinite fluid, such as the ocean.

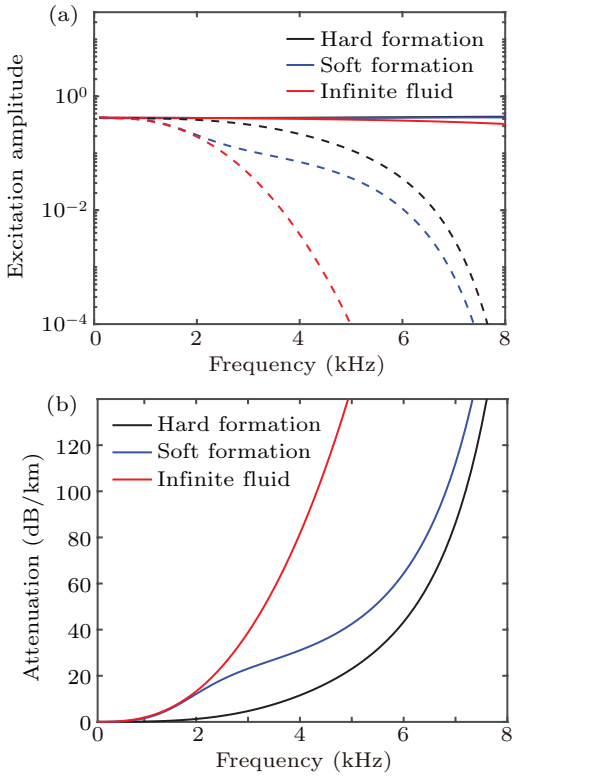


Fig. 4. Excitation and attenuation spectra of the drill-string wave in three cases. (a) Comparisons of excitation spectra for two selected receiver-to-source offsets at $z_0 = 3$ m (solid lines) and $z_0 = 500$ m (dashed lines), and (b) attenuation curves.

Table 2. Records of attenuation values (dB/km) at selected frequencies.

	1 kHz	3 kHz	5 kHz
Hard formation	0.14	4.70	23.01
Soft formation	1.57	23.10	42.47
Infinite fluid	1.92	38.81	145.20

With discussions of the excitation and attenuation characteristics of the drill-string wave in the borehole, the transmission coefficient can be calculated by Eq. (11). Figure 5 shows the calculation results of the 20-section drill string with tool joint 1 listed in Table 1. It is illustrated that the passband amplitudes corresponding to the infinite fluid case decay the most as the frequency increases, which is consistent with the results of attenuation curves. In addition, the bandgap distributions of

drill-string waves are the same for the three transmission environments; that is, changes in the surrounding medium parameters do not cause the bandgaps of the drill-string wave to shift. These results suggest that the available carrier bandwidth depends mainly on the transmission environment by linking to the communication system. Figure 5 reveals the coupling effect of the drill-string wave with the periodic tool joints and the radial waveguide. Further, combined with the noise data in the field, the channel function provided by Eq. (11) can be used as the basis for channel estimation and channel capacity evaluation.

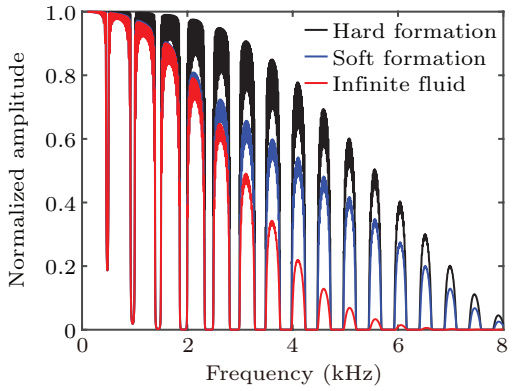


Fig. 5. Transmission coefficients of the drill-string wave for three waveguides.

3.2. Synthetic wavefields of numerical model

Finite-difference time-domain (FDTD) algorithm is the standard method for synthesizing borehole wavefields.[23,24] With the velocity-stress staggered grid FDTD in the cylindrical coordinates, to guarantee the stability conditions, the space grid step size Δr or Δz should satisfy $\Delta r, \Delta z \leq V_{\min}/10f_{\max}$, where $V_{\min}$ is the minimum velocity of the medium in the whole radial space and $f_{\max}$ is the maximum frequency, and the time step needs to meet $\Delta t \leq \Delta r/\sqrt{2}V_{\max}$, where $V_{\max}$ is the maximum velocity of all media.[25–27]

The numerical model of the DAT is designed to be 40 m long with absorption boundaries at both ends. Receivers are still mounted on the inner surface of the drill string. Before the simulations, to verify the accuracy of the FDTD program, we compare the received waveforms for the uniform cylindrical waveguide, which are calculated by FDTD and individual wave arrivals, respectively, as shown in Fig. 6. Individual waveforms are obtained by evaluating Eq. (4). The numerical model is a hard formation borehole and the medium parameters are listed in Table 1. The source function is the cosine envelope pulse with a central frequency of 4 kHz, and its specific expression is given by Cui.[15] Four selective receiver-to-source offsets are labeled in Fig. 6. It can be seen that the waveforms simulated by FDTD coincide with those calculated by the analytic method well, thus proving the accuracy of numerical simulations.

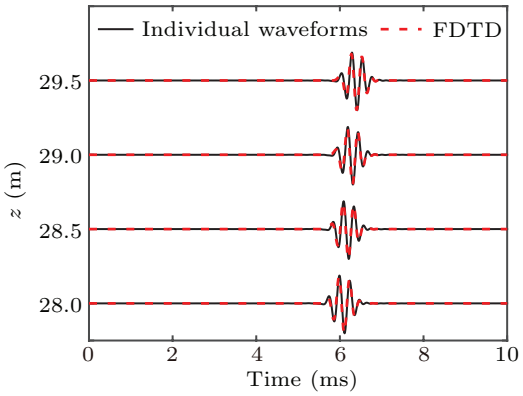


Fig. 6. Comparisons of the waveforms simulated by FDTD and individual wave arrivals with the central frequency of 4 kHz in a hard formation.

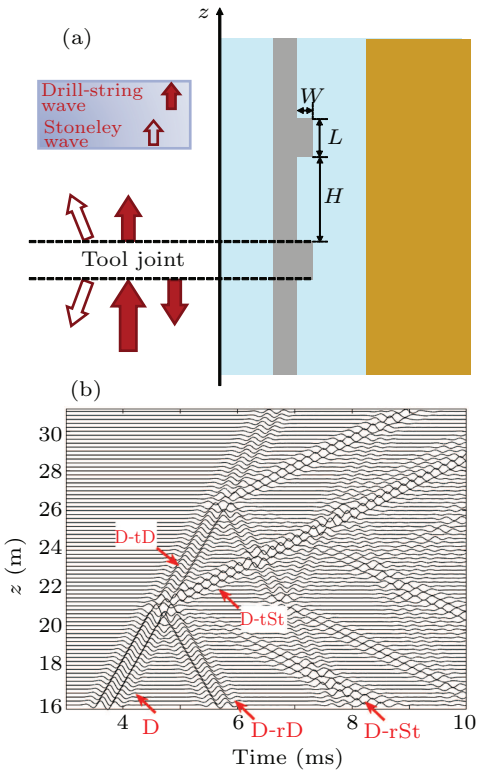


Fig. 7. Two-tool-joint drill string: (a) schematic diagram of wave motion, where L, W, and H denote the tool joint length, the tool joint width, and the pipe length, respectively. (b) Recorded waveforms from $z = 16$ m to $z = 31$ m at the inner surface of the drill string. The time is not recorded from zero.

For the first numerical model, we design a two-tool-joint drill string with tool joint 1 listed in Table 1. As shown in Fig. 7(a), the drill string parameters labeled are $L = 0.2$ m, $W = 0.01$ m, and $H = 5$ m, respectively. Such a simple model can help us to focus on the path of wave motion. Figure 7(b) presents the received waveform array on the inner surface of the drill string from $z = 16$ m to $z = 31$ m with an equal interval of 0.2 m. The offsets noted by the vertical coordinate correspond to the drill-string schematic. In Fig. 7(b), the upgoing wave labeled as 'D' is the direct drill-string wave. When encountering the first tool joint ($z \approx 21$ m), part of the drill-string wave reflects due to the impedance discontinuity of the tool joint. In addition, except for the reflected drill-string wave

(D-rD) and the transmitted drill-string wave (D-tD), two additional waves are generated in the recorded wavefield. To confirm these new waves, we apply the slowness-time coherence (STC) algorithm[28] to analyze the slowness of each wavelet in the full-wave arrays. Note that STC is a valid processing technique only if there is minimal dispersion. Figure 8(a) presents the semblance processing for the full waveforms received from $z = 28$ m to $z = 29.5$ m in the time-slowness domain. According to the slowness plot in Fig. 8(a), the new waves can be confirmed as converted Stoneley waves. It indicates that the tool joint acts as a scattering source that interferes with the original wavefield in the borehole. From Fig. 7(b), the converted Stoneley wave also separates the reflected part (D-rST) and the transmitted part (D-tSt). This mode conversion phenomenon can also be observed at the second tool joint ($z \approx 27$ m).

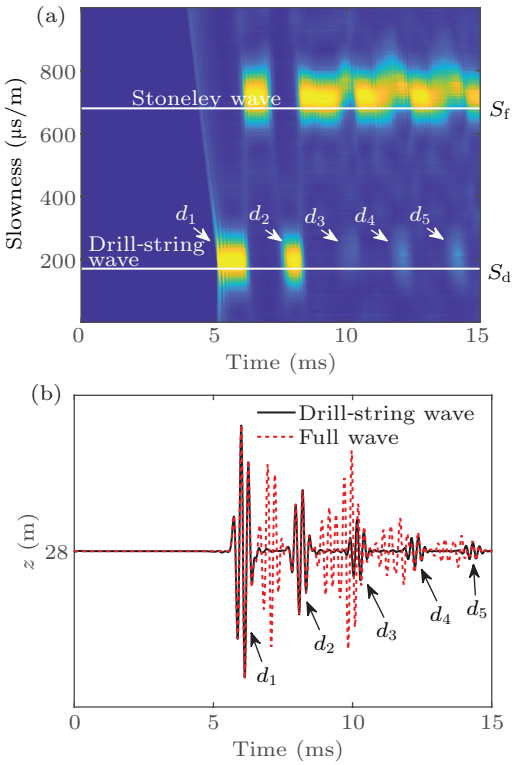


Fig. 8. Two-tool-joint drill string: (a) time-slowness diagram for the full waves. S_d and S_f indicate the drill-pipe and fluid slowness, respectively; d_1–d_5 indicate the five successive arrivals of the drill-string wave. (b) The separation of the full waves and the drill-string waves at receiver-to-source offset $z = 28$ m.

Figure 8 presents that the drill-string wave arrives in several groups d_1–d_5 caused by the multiple-reflection effect. The last three groups are swamped by the strong and long-duration Stoneley waves. To distinguish each mode wave, we separate the drill-string waves from the full waveforms by applying the frequency-wavenumber (F-K) filtering technique. As shown in Fig. 8(b), the black line represents the separated drill-string wave, and the dotted red lines represent the original full waveform. Five distinct groups d_1–d_5 of the drill-string wave can be observed, and the trajectory of the drill-string wave and the converted Stoneley wave become distinguished. Figure 9 presents the comparison of the synthetic drill-string waveforms calculated by Eq. (12) with that calculated by the FDTD method. It can be seen from the figure that the two waveforms match well, which validates that the modeling method proposed in this study can accurately describe the propagation of the drill-string wave. The wavefield synthesized by the FDTD method cannot be used to calculate the channel function because it fails to contain the full travel time information. The propagation matrix method is evaluated in the frequency domain and has great advantages in computational efficiency, so it is more suitable for DAT modeling. However, the converted Stoneley waves also have strong amplitudes, as seen in the wavefield synthesized by the FDTD method. In the next section, we will discuss the factors influencing the conversion intensity and observe the phenomenon of bandgap shifts.

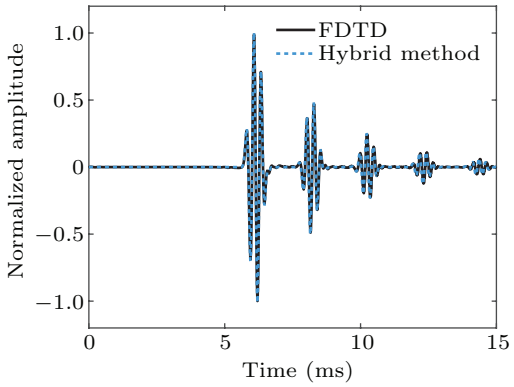


Fig. 9. Comparison of the synthetic waveforms calculated by the proposed hybrid method with those calculated by the FDTD method.

3.3. Conversion intensity and bandgap variations

To investigate the interactions between the converted intensity of the drill-string wave and the propagation environments, we still use the two-tool-joint drill string model, as shown in Fig. 7(a), and change the formation properties and tool-joint radii. The FDTD method is used to simulate wavefields in five cases and to compare the received waveforms at $z = 28$ m, as shown in Figs. 10(a) and 10(b). The labels HF, SF, and IF in the legends denote hard formation, soft formation, and infinite fluid, respectively; TJ1, TJ2, and TJ3 correspond to the three types of the tool joint listed in Table 1. The case of HF-TJ1 is used as a reference in two figures. With the same type of tool joint, waveforms in Fig. 10(a) reflect the effect of surrounding formation on the mode conversion. Figure 10(b) compares the cases of different tool joints while the hard formation is outside the borehole. According to Table 1, the material parameters of the three tool joints are the same, so the wave impedance of the tool joint is only proportional to the cross-sectional area. Each received waveform presents two wave arrivals, where the first arrival is the transmitted drill-string wave, and the second one is the converted Stoneley

wave. For a more straightforward comparison, we define the relative conversion intensity ε as the ratio of the energy of the transmitted drill-string wave to the converted Stoneley wave as

$$\varepsilon = \frac{\int_{T_2} |s(t)|^2 \, \mathrm{d}t}{\int_{T_1} |s(t)|^2 \, \mathrm{d}t}, \tag{14}$$

where $s(t)$ is the amplitude of the received waveform; T_1 and T_2 denote time ranges of the transmitted drill column wave and the converted Stoneley wave, as labeled in Figs. 10(a) and 10(b). The results calculated by Eq. (14) are presented in Fig. 10(c). It is demonstrated that the relative conversion intensity of the drill-string wave is positively correlated not only with the cross-sectional area of the tool joint but also with the wave impedance of the outer formation. Hard formation outside the borehole intensifies the conversion of drill-string waves to Stoneley waves, and the opposite is true for the drill string in an infinite fluid.

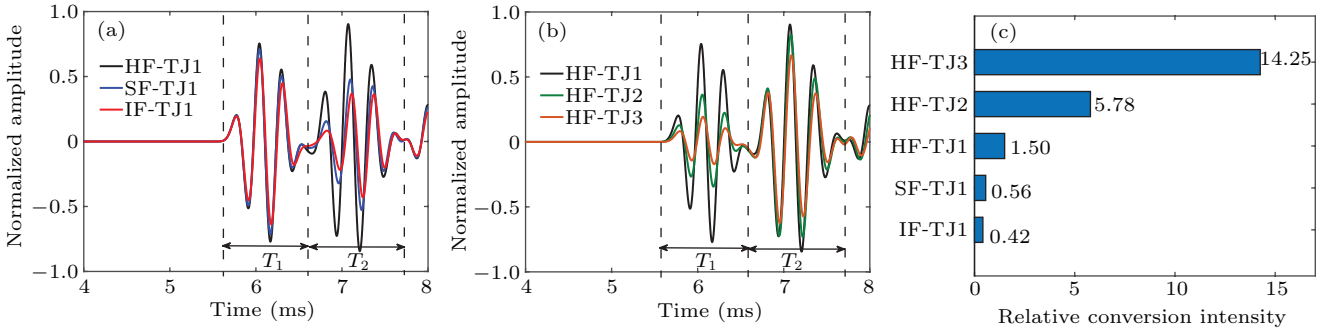


Fig. 10. Two-tool-joint drill string: comparisons of the waveforms received at $z = 28$ m for variations of (a) propagation environments and (b) tool joint radii, and (c) calculations of the relative conversion intensity. The labels HF, SF, and IF denote hard formation, soft formation, and infinite fluid, respectively; TJ1, TJ2, and TJ3 correspond to the three types of the tool joint listed in Table 1.

Finally, we design a five-tool-joint model with hard formation and tool joint 1. The synthesized waveforms are received at the receiver-to-source offset $z = 28$ m and are calculated by the inverse Fourier transform to evaluate the frequency-domain responses. Figure 11 compares the frequency-domain responses of the drill-string wave, calculated by the FDTD and the proposed hybrid method, respectively. It can be observed that the bandgap distributions calculated by the two methods are consistent. In addition, the amplitudes of each passband coincide well except for the first and last passbands, which is due to the weak energy of the modulated waveform at high and low frequencies. This result further validates that the proposed hybrid method is capable of predicting the bandgap distribution when no conversion effect is involved. Then, in order to investigate the interference of the converted Stoneley waves on the bandgap distribution, we compare the spectra of the drill-string wave and full wave simulated by the FDTD method, as shown in Fig. 12. Under the influence of the mode-conversion effect, some passbands of the channel exhibit frequency-selective decay characteristic. This finding means that the carrier passing through the channel will face additional amplitude distortion. Moreover, from Fig. 12, although some passbands shift and split, the periodic bandgap characteristic can still be identified in the frequency response. Therefore, the theoretical channel function is still necessary and practically useful. It is of more concern how to ensure the reliability of the DAT system in transmitting data. For example, we can counteract the variation of bandgap distribution by employing a multi-baseband carrier scheme, as carried out by Zheng *et al.*[14] This study will provide the theoretical basis for the design of the DAT system.

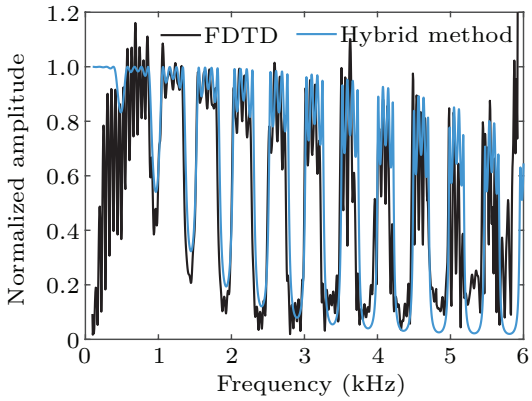


Fig. 11. Comparison of the frequency-domain responses of the drill-string wave calculated by the proposed hybrid method with that calculated by the FDTD method.

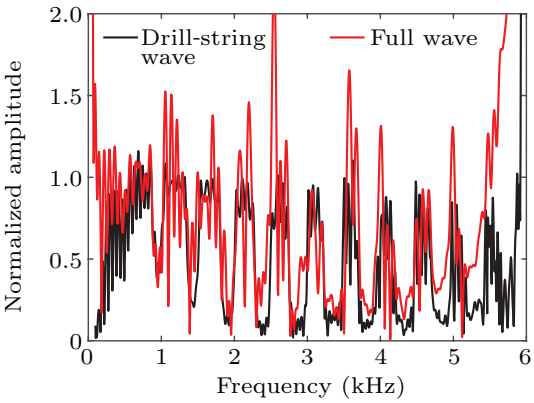


Fig. 12. Spectrum comparison of the drill-string wave with the full wave.

4. Conclusion and perspectives

In summary, we focus on the response characteristics of the drill-string guided wave in DAT and propose a hybrid modeling algorithm to evaluate the channel function. The conclusion and perspectives are provided as follows.

(i) The hybrid method provides channel functions which include transmitting and receiving deployments, periodicity of the structure, and radial waveguide property. This method has high computational efficiency, and its effectiveness is confirmed through comparison with the existing finite-difference method.

(ii) In order to obtain stronger drill string waves, the suitable transmitting and receiving deployment of the DAT is determined. An axisymmetric shear-stress source is applied to the outer wall of the drill pipe while the receiving array is placed in the inner fluid layer. It is demonstrated that the excitation characteristics near the source are hardly affected by the formation property.

(iii) The coupling of the attenuation and conversion intensity of the drill-string wave with the surrounding medium is quantitatively studied. We reveal that outermost media with large acoustic impedance can significantly reduce the leakage of wave energy while intensifying the conversion of drill-string waves to Stoneley waves. Conversely, the attenuation of drill-string waves in infinite fluids is large, and the conversion effect is weak. In addition, the conversion intensity of the drill-string wave is positively correlated to the cross section of the tool joint.

(iv) The impact of the drill-string-wave conversion effect on the bandgap distribution is illustrated. Although some passbands of the channel exhibit frequency-selective decay caused by the converted Stoneley waves, the periodic bandgap characteristic can still be identified. For the problem of guided wave interference in solid channels, it is of general interest to improve the reliability of communication systems to combat the additional introduction of amplitude distortion.

This study not only provides a more effective modeling method for the DAT but also enriches the understanding of the general solid-state acoustic channel.

Acknowledgements

Project supported by the National Natural Science Foundation of China (Grant Nos. 11734017 and 12174421), and the Scientific Instrument Developing Project of the Chinese Academy of Sciences (Grant Nos. YJKYYQ20200072 and GJJSTD20210008).

References

[1] Tochikawa T, Sakai T, Taniguchi R and Shimada T 1996 *Proceedings of SPE Annual Technical Conference and Exhibition*, October 6–9, 1996 Denver, USA, paper number: SPE-36433-MS
[2] Shah V, Gardner W, Johnson D H and Sinanovic S 2004 *Proceedings of SPE Asia Pacific Oil and Gas Conference and Exhibition*, October 18–20, 2004 Perth, Australia, paper number: SPE-88636-MS
[3] Neff J M and Camwell P L 2007 *Proceedings of SPE/IADC Drilling Conference*, February 20–22, 2007 Amsterdam, Netherlands, p. 105021
[4] Reeves M E, Camwell P L and Mcrory J 2011 *Proceedings of SPE Offshore Europe Oil and Gas Conference and Exhibition*, September 6–8, 2011 Aberbeen, UK, paper number: SPE-145566-MS
[5] Drumheller D S 1989 *J. Acoust. Soc. Am.* **85** 1048
[6] Drumheller D S 1993 *J. Acoust. Soc. Am.* **94** 2387
[7] Drumheller D S and Knudsen S D 1995 *J. Acoust. Soc. Am.* **97** 2116
[8] Lee H Y 1991 *Drillstring axial vibration and wave propagation in boreholes* (Ph.D. dissertation) (Cambridge: Massachusetts Institute of Technology)
[9] Rama Rao V N and Vandiver J K 1999 *J. Acoust. Soc. Am.* **105** 3057
[10] Lous N J S, Rienstra S W and Adan I J B F 1998 *J. Acoust. Soc. Am.* **103** 2302
[11] Wang C Y, Qiao W X and Zhang W Q 2006 *Proceedings of IEEE International Symposium on Signal Processing and Information Technology*, October 27–30, 2006 Vancouver, Canada, p. 415
[12] Carcione J M and Poletto F 2000 *J. Acoust. Soc. Am.* **108** 53
[13] Gutierrez-Estevez M A, Krueger U, Krueger K A, Manolakis K, Jungnickel V, Jaksch K, Krueger K, Mikulla S, Giese R, Sohmer M and Reich M 2013 *Proceedings of IEEE Wireless Communications and Networking Conference*, April 7–10, *2013* Shanghai, China, p. 4089
[14] Zheng L C, Yu J Q, Yang Q H, Gao Y and Sun F C 2017 *Petro. Explor. Develop.* **44** 321
[15] Cui Z W 2004 *Theoretical and numerical study of modified biot's models, acoustoelectric well logging and acoustic logging while drilling excited by multipole acoustic sources* (Ph.D. dissertation) (Changchun: Jilin University) (in Chinese)
[16] Sinha B K, Simsek E and Asvadurov S 2009 *Geophysics* **74** E111
[17] Zheng X B and Hu H S 2017 *Geophysics* **82** D1
[18] He X, Wang X M and Chen H 2017 *Wave Motion.* **72** 287
[19] Yang Y F, Guan W, Hu H S and Xu M Q 2017 *Geophys. J. Int.* **209** 749
[20] Kurkjian A L and Chang S K 1986 *Geophysics* **51** 148
[21] Saniie J, Wang B Y and Xin H 2018 *Proceedings of IEEE International Ultrasonics Symposium*, October 22–25, 2018 Kobe, Japan pp. 1–10 (invited paper)
[22] Kurkjian A L 1985 *Geophysics* **50** 852
[23] Yee K S 1966 *IEEE Trans. Antennas and Propagation.* **14** 302
[24] Leslie H D and Randall C J 1992 *J. Acoust. Soc. Am.* **91** 12
[25] Stephan R A, Cardo-Casas F and Cheng C H 1985 *Geophysics* **50** 1588
[26] Virieux J 1986 *Geophysics* **51** 889
[27] Liu Q H, Schoen E, Daube F, Randall C, Liu H L and Lee P 1996 *J. Acoust. Soc. Am.* **100** 72
[28] Kimball C V and Marzetta T L 1984 *Geophysics* **49** 274